Aust. J. Phys., 1994, **47**, 1–23

Studies Involving the Resonant Interaction of Laser Light with Atoms

W. R. MacGillivray and M. C. Standage

Laser Atomic Physics Laboratory, School of Science,
Griffith University, Nathan, Qld 4111, Australia.

Abstract

In this article, we review three areas of study in which the resonant interaction between atoms and laser radiation plays a central role. Firstly, coherent optical transients are discussed in which the direct observation of this interaction can be studied via the detection of the Rabi frequency in optical nutations. Secondly, the response of atoms to resonant radiation in an optical cavity leading to optical bistability and other effects is described. Finally, the new field of atom manipulation by resonant laser fields is introduced, in particular, the deflection of atomic beams. The underlying theoretical framework for the experiments performed is discussed, ranging from full quantum electrodynamic to semiclassical models.

1. Introduction

Narrow bandwidth, single mode, tunable dye lasers were developed and commercialised two decades ago. Their widespread availability caused a resurgence in activity in the area of atomic spectroscopy. However, not only was it now possible to obtain spectra of very high resolution, it was also feasible to study coherence effects in atom–light interaction.

This revolution in experimental methods has forced a commensurate change in theoretical approaches. With conventional non-laser light sources, it was generally assumed that, at most, only one photon interacted with an atom during the lifetime of an atomic excited state. Such a weak excitation allowed perturbation theory to be applied. Even if more than one photon was involved, they were not coherently related and rate equations were sufficient to describe the system.

To include the coherence effects in a theoretical description requires the ability to handle superposition states. Models involving the density operator achieve this but, even though the Hamiltonian describing the atom and the atom–light interaction is quantum-mechanical, the light field is treated classically. This leads to an absence of the non-coherent relaxation terms which must then be included on an ad hoc basis. This process is relatively straightforward for simple atomic systems of two or three energy states, but it is not feasible when there are more states than this. It was for this reason that even complex atomic transitions such as the D_2 line of sodium in hyperfine representation, which has a total of 24 magnetic substates, were, by approximation, described by two or three states. At times, the number of states participating in an interaction can be reduced by some preparation. For example, optical pumping of the sodium D_2

0004-9506/94/010001$05.00

hyperfine transition $3^2S_{1/2}(F=2)$–$3^2P_{3/2}(F=3)$ by circularly polarised light can achieve a two-state system, $3^2S_{1/2}(F=2, m_F=2)$–$3^2P_{3/2}(F=3, m_F=3)$. However, it is not always possible or desirable to effect this pumping in an experiment. Theoretical models employing a fully quantum-mechanical representation for the atom, field and their interaction are now available for a complete description of atom excitation by resonant laser radiation.

In this review article, we shall discuss three topics involving laser–atom interactions; namely, coherent optical transients, optical bistability and atom manipulation. The interrelationships between the topics and, in particular, the underlying theoretical development will be emphasised.

2. Coherent Optical Transients

Probably the most fundamental manifestation of the coherent interaction between laser radiation and an atomic transition is Rabi cycling (Knight and Allen 1983). This phenomenon is best described by considering an atomic transition between two isolated states, the lower of which is the ground state, $|g\rangle$. When the atom is exposed to a near-resonant monochromatic field, the excitation probability as a function of time is of harmonic form with a frequency of $(\Omega^2+\Delta^2)^{1/2}$, where Δ is the frequency detuning of the radiation from the transition and Ω is the on-resonance Rabi frequency associated with the transition. The Rabi frequency is a measure of the strength of interaction between the radiation field $\boldsymbol{E}$ and the induced atomic dipole $\boldsymbol{D}$ and is defined as

$$\Omega = -\boldsymbol{D}.\boldsymbol{E}/\hbar. \tag{1}$$

The physical interpretation of the excitation probability is that the individual atom, initially in the ground state, is excited to the upper state $|e\rangle$ by the absorption of a photon from the radiation field, and then is stimulated to return to the ground state, also by its interaction with the field. Once back in the ground state, the atom is re-excited and the cycle continues. Thus an individual atom experiences a coherent optical cycling interrupted randomly by incoherent events such as spontaneous emission or collisions.

Formally, the macroscopic polarisation of an ensemble of atoms subjected to a coherent laser field is given by

$$\boldsymbol{P} = N\,\mathrm{tr}(\rho\boldsymbol{D}), \tag{2}$$

where N is the atomic number density and ρ the density operator. The amplitude $E(z,t)$ of the scattered field is related to the amplitude $P(z,t)$ of the polarisation by Maxwell's wave equation which is given, in the slowly varying amplitude approximation, by (Allen and Eberly 1975)

$$\frac{\partial}{\partial z}E(z,t) + \frac{1}{c}\frac{\partial}{\partial t}E(z,t) = \frac{\mathrm{i}\omega_L}{2c\epsilon_0}P(z,t), \tag{3}$$

where z is the direction of radiation propagation and ω_L the radiation frequency.

By considering the macroscopic polarisation of a medium of two-level atoms suddenly switched into resonance with a single-mode laser field, it can be

shown that the field amplitude scattered by the atoms in the forward direction (coherent scattering) will exhibit Rabi oscillations (Brewer 1975). 'Suddenly' is here measured on the time scale of the upper state lifetime which for atoms is typically of the order of 10 ns. The oscillations persist for only a few lifetimes as the dephasing of the coherent signal from the ensemble is achieved by the non-coherent relaxation of individual atoms. Indeed, even in the absence of an incoherent relaxation process, the Boltzmann distribution of atomic velocities in the medium, which gives rise to a distribution in the detuning frequency from the Doppler effect, causes a dephasing of the oscillatory signal which takes on the form of the Bessel function of the first kind, J_0. This oscillatory signal is often referred to as an optical nutation.

Brewer and Shoemaker (1971) demonstrated how the forward-scattered field amplitude could be detected in the presence of a laser field using a heterodyne method when they observed Rabi oscillations in optical nutations from molecular transitions. The molecules were Stark-shifted into resonance with radiation from a CO_2 laser by the sudden application of an electric field. We adapted this experimental technique to the study of Na atoms where the requirements for the voltage pulse were more severe with the need to apply an electric field of the order of 100 $\mathrm{kV\,cm^{-1}}$ in a time of the order of 1 ns.

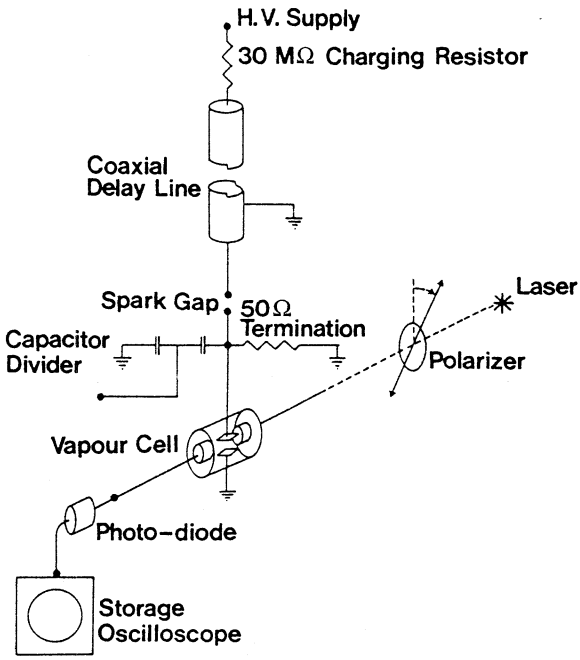

Fig. 1. Schematic diagram of the apparatus used for the detection of coherent optical transients. [From MacGillivray *et al.* (1978).]

A schematic diagram of the apparatus used for the detection of optical nutations in atomic Na is shown in Fig. 1 (MacGillivray *et al.* 1978). The high voltage pulsing unit consisted of a supply, a delay line, a coaxial pressurised spark gap

and a matched termination. This unit produced voltage pulses of up to 20 kV amplitude with rise times of approximately 1 ns and durations 60 ns, which were applied to platinum electrodes spaced 1·9 mm apart inside a glass cell. The cell was filled with Na which was heated to form a vapour. The intensity profile of the linearly polarised, single-mode, cw laser beam was Gaussian with a 1/e diameter of about 2 mm. The laser was tuned to the D_2 line of Na. The transmitted beam was detected by a PIN photodiode after passing through an aperture which excluded all but the uniform central region. The output of the photodiode was monitored by a storage oscilloscope which was triggered by the applied voltage

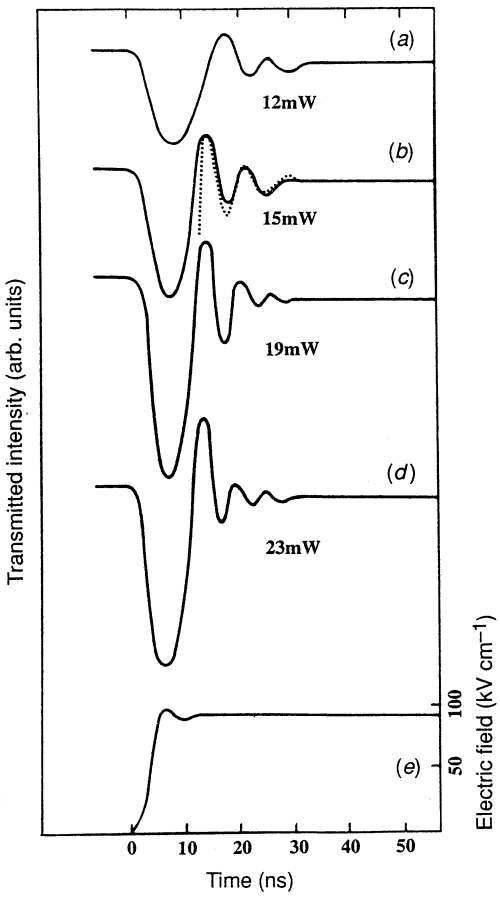

Fig. 2. Optical nutation data for various values of laser intensity expressed as total power in a 2 mm diameter Gaussian profile beam. The corresponding values of the deduced Rabi frequency for each curve are (*a*) 127 MHz, (*b*) 140 MHz, (*c*) 165 MHz and (*d*) 180 MHz. The dotted curve in (*b*) is from the calculation of a two-state density matrix model normalised to the first maximum (see text for details). Curve (*e*) is the applied electric field pulse. [From MacGillivray *et al.* (1978).]

pulse. The enhanced signal-to-noise ratio of the heterodyne signal enabled single-shot recording of the data. Owing to the heterodyning method used, the slowly varying part of the transmitted light intensity detected is proportional to the real part of the scattered field amplitude E. For an ensemble of two-state atoms, the scattered field can be determined from equations (2) and (3) yielding, for the heterodyne signal,

$$\mathrm{Re}[E(t)] = CD_{12}\,\mathrm{Im}[\tilde{\rho}_{12}(t)]_{\mathrm{av}}\,, \tag{4}$$

where C is a constant for the atomic species, D_{12} is the relevant dipole matrix element and the imaginary part of the slowly varying density matrix element, $\tilde{\rho}_{ij}$, defined by

$$\rho_{ij} = \tilde{\rho}_{ij} \exp[\mathrm{i}(\omega_L t - kz)], \tag{5}$$

is averaged over the velocity profile of the atoms in the ensemble. The density matrix element can be determined from the solution of the component equations derived from the density operator equation of motion (Allen and Eberly 1975)

$$\dot{\rho} = -\frac{\mathrm{i}}{\hbar}[H, \rho] + \text{relaxation terms}, \tag{6}$$

where H is the semiclassical Hamiltonian and the relaxation terms are added in an ad hoc manner.

Fig. 2 exhibits typical data. The oscillatory features are due to the scattered field amplitude and are optical nutations. At switch-on of the voltage pulse, the transmitted intensity decreases rapidly due to the absorption of photons as the atoms in the ensemble are excited to the upper state. Then follows an increase in the intensity above its steady-state value as photons are coherently emitted from the atoms due to stimulated emission. This cycle continues but is rapidly damped out due to the processes discussed above. Apparent in the data is the increase in the Rabi frequency of the optical nutation as the intensity is increased. From equation (1), it can be seen that the Rabi frequency is proportional to the square root of the intensity. We have subsequently observed optical nutation

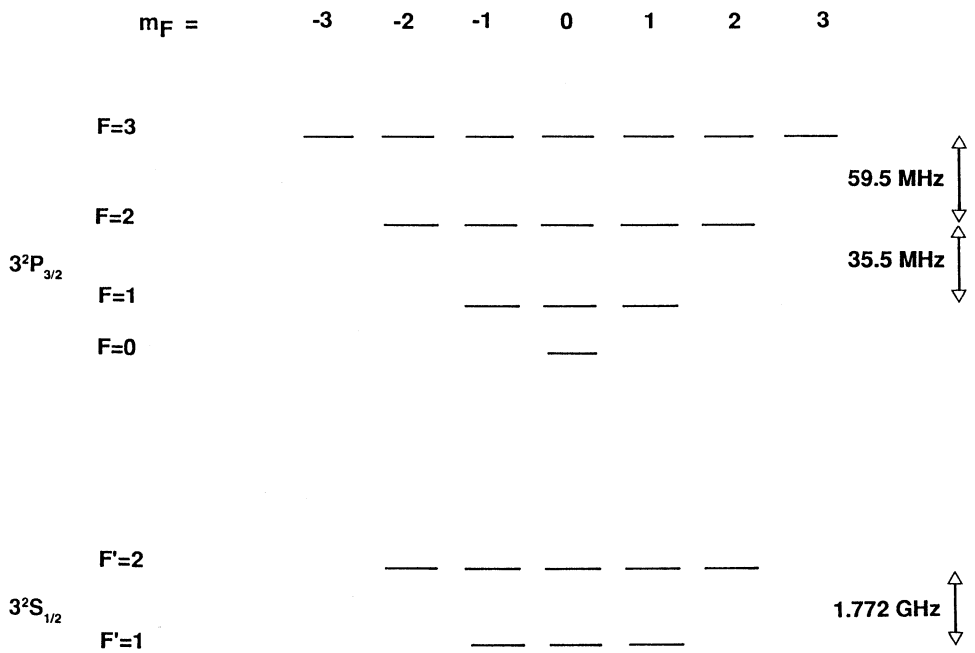

Fig. 3. Energy states, in hyperfine representation, associated with the D_2 line of sodium.

signals in the Na D lines both from an atomic vapour and a multiple atomic beam system by using an electro–optic switch to create a rectangular light pulse from the cw laser radiation (Farrell *et al.* 1985; Schulz *et al.* 1989).

Plotted on curve (*b*) of Fig. 2, and normalised to the first maximum of the experimental data, is a theoretical curve computed from the two-state semiclassical density operator theory of equation (4). That a two-state theory should give good agreement was somewhat of a surprise considering the energy level structure associated with the D_2 line of Na in hyperfine representation, as illustrated in Fig. 3. Subsequent Fourier analysis of the data indicated that the optical nutations consisted of essentially a single Rabi frequency. The Rabi frequency associated with each of the hyperfine transitions in the D_2 manifold can be written as (Farrell *et al.* 1994)

$$\Omega_{Fm_F,F'm_{F'}} = \left(\frac{6\pi c^2 \Gamma_{\rm eg}}{\hbar\omega_{\rm eg}^3}\right)^{\frac{1}{2}} C(Fm_F,\, F'm_{F'},\, L,\, L')I^{\frac{1}{2}}\,, \tag{7}$$

Table 1. Values of $C(Fm_F, F'm_{F'}, L, L')$ of equation (7) for the π excitation of the hyperfine transitions $3^2S_{\frac{1}{2}}(F{=}2)$–$3^2P_{\frac{3}{2}}(F{=}3,2,1)$

m_F	−3	−2	−1	0	1	2	3
$F{=}3$		$-1/\sqrt{3}$	$-4/\sqrt{30}$	$-3/\sqrt{15}$	$-4/\sqrt{30}$	$-1/\sqrt{3}$	
$F{=}2$		$1/\sqrt{3}$	$1/\sqrt{12}$		$-1/\sqrt{12}$	$-1/\sqrt{3}$	
$F{=}1$			$1/\sqrt{20}$	$1/\sqrt{15}$	$1/\sqrt{20}$		

where F is the total angular momentum quantum number in hyperfine representation and L is the orbital quantum number for each state. The prime indicates a substate of state $|{\rm g}\rangle$, while $\omega_{\rm eg}$ is the transition frequency, $\Gamma_{\rm eg}$ the relaxation rate between the two states, and I the radiation intensity. The coefficient $C(Fm_F, F'm_{F'}, L, L')$ consists of angular momentum vector addition coefficients derived from reducing the dipole matrix element from F representation to a common reduced matrix element in L representation. If we assume that the ground states can be resolved by the narrow-band laser radiation, π excitation from the $3^2S_{\frac{1}{2}}(F{=}2)$ state to the $3^2P_{\frac{3}{2}}(F{=}3,2,1)$ states consists of twelve hyperfine transitions. The constants $C(Fm_F, F'm_{F'}, L, L')$ for these transitions are given in Table 1 where it is apparent that they have a wide range of values. Calculation of the optical nutation signal for this system is via a straightforward generalisation of equation (4) and is given by

$$\mathrm{Re}[E(t)] = C\sum_{\rm eg} D_{\rm eg}\,\mathrm{Im}[\tilde{\rho}_{\rm eg}(t)]_{\rm av}\,, \tag{8}$$

where the sum is over all the optical coherences formed between the substates of $|{\rm e}\rangle$ and $|{\rm g}\rangle$. However, the derivation of the component equations for the density matrix is not straightforward because of the difficulty in determining the relaxation terms. Rather, we have generalised the atomic operator method introduced for two-state systems (Ackerhalt *et al.* 1973; Ackerhalt and Eberly 1974) in which the relaxation terms arise naturally from the quantum treatment of

the field. This is a fully quantum-electrodynamic theory for the atomic operator σ whose time evolution is governed by the Heisenberg equation of motion

$$\dot{\sigma} = -\frac{\mathrm{i}}{\hbar}[\sigma, H], \tag{9}$$

where the Hamiltonian in the Heisenberg representation is fully quantum-mechanical and the operator elements are given by

$$\sigma_{ij} = |i\rangle \langle j|. \tag{10}$$

The details of the derivation of the component equations for a general non-degenerate two-level system can be found elsewhere (Farrell *et al.* 1988). As is the case with the density matrix elements, the component equations for the atomic operator are derived in terms of the slowly varying element, χ_{ij}

$$\sigma_{ij} = \chi_{ij} \exp[-\mathrm{i}(\omega_L t - kz)], \tag{11}$$

where kz is the phase due to propagation in the z direction. Recognising the relationship between the atomic operator and density matrix elements as

$$\langle \chi_{ij}(t) \rangle = \tilde{\rho}_{ji}(t) \tag{12}$$

leads to the recasting of equation (8) as

$$\mathrm{Re}[E(t)] = C \sum_{\mathrm{eg}} D_{\mathrm{eg}} \, \mathrm{Im}[\chi_{\mathrm{ge}}(t)]_{\mathrm{av}}. \tag{13}$$

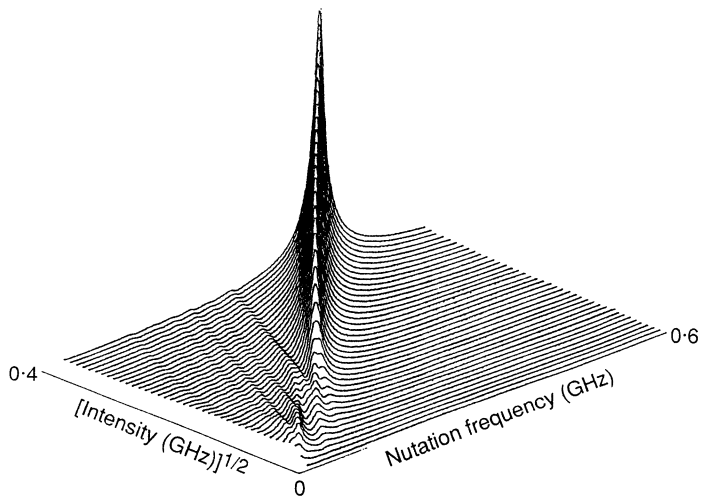

Fig. 4. Fourier transforms of the optical nutation signals calculated for the π excitation of the $3^2S_{1/2}(F{=}2)$–$3^2P_{3/2}(F{=}3,2,1)$ hyperfine transitions of sodium. The signals are plotted as a function of the square root of the radiation intensity expressed as the Rabi frequency of the $3^2S_{1/2}(F{=}2, m_F{=}0)$–$3^2P_{3/2}(F{=}3, m_F{=}0)$ transition. [From MacGillivray *et al.* (1990).]

Equation (13) has been evaluated for the π excitation of the $3^2S_{1/2}(F=2)$ to $3^2P_{3/2}(F=3,2,1)$ transitions of Na without the averaging over the atomic velocity profile (MacGillivray *et al.* 1990). The averaging makes no qualitative difference to the computed signals. In Fig. 4 the Fourier transforms of the optical nutation signals are plotted as a function of the square root of the radiation intensity expressed as the Rabi frequency of the $3^2S_{1/2}(F=2, m_F=0)$ to $3^2P_{3/2}(F=3, m_F=0)$ hyperfine transition. As can be observed from the plot, at low intensities there are a number of frequency components which would give rise to a complicated optical nutation signal. However, by the time that the intensity scale reaches 150 MHz (about 40 $\mathrm{mW\,mm^{-2}}$) the signal has collapsed to a single frequency. That the calculations of a two-state model fitted the experimental data of Fig. 2 at 140 MHz is explained by the results of Fig. 4 since, at this nutation frequency, the signal does consist of essentially one frequency due to the interference between all of the component Rabi frequencies.

Another demonstration of Rabi cycling was observed in a different experiment (Murray *et al.* 1991) in which mercury atoms were stepwise excited by inelastic electron collisions followed by resonant laser interaction. Fig. 5 is a schematic of the stepwise process. Stimulated absorption and emission cycles are possible in the laser excitation of the 6^1P_1–6^1D_2 transition. Coincidences between the scattered electrons and photons from the 6^1D_2–6^3P_1 channel were detected, yielding a time-resolved intensity signal as shown in Fig. 6. While no oscillations are apparent in this signal which would indicate Rabi cycling, it was noted that the decay time of the signal, which measures the laser-excited state lifetime, was $5{\cdot}8\pm1$ ns, corrected for radiation trapping effects. The accepted lifetime value for the 6^1D_2 state is $10{\cdot}9$ ns. The reduction in the decay time can be explained as the first full Rabi cycle, that is, one cycle of absorption and stimulated emission. No further cycles were observed in this signal since the lifetime of the 6^1P_1 state is only $1{\cdot}3$ ns, and so there is a much greater probability at this laser intensity that the atoms will relax back to the ground state rather than being re-excited to the 6^1D_2 state. A calculation of the time-resolved signal using the full QED model was in good agreement with the observed data for a laser intensity of 60 $\mathrm{mW\,mm^{-2}}$. An experiment is being planned where the electron-excited state will be a metastable state allowing for many Rabi cycles in the laser-excited transition. Under these circumstances, Rabi oscillations should be apparent in the time-resolved coincident fluorescence signal.

Other phenomena that are classified as coherent optical transients include photon echoes and free induction decay (FID). The latter effect was studied using the same apparatus as used for the optical nutation experiments described above. Whereas the optical nutation signal is generated from atoms switched into resonance with the laser radiation, atoms switched out of resonance produce the FID signal in the forward scattered direction as they relax back to their equilibrium condition. As for the optical nutation, the FID signal is phase-related to the laser radiation and so can be detected by the same heterodyning method. For two-state atoms, the scattered field amplitude is observed as the slowly varying component of the detected intensity, as given in equation (4). However, in this case, the density matrix component is calculated from the equations of motion with the Rabi frequency term put to zero and with the steady-state solution as the initial conditions. This model reflects the conditions that the

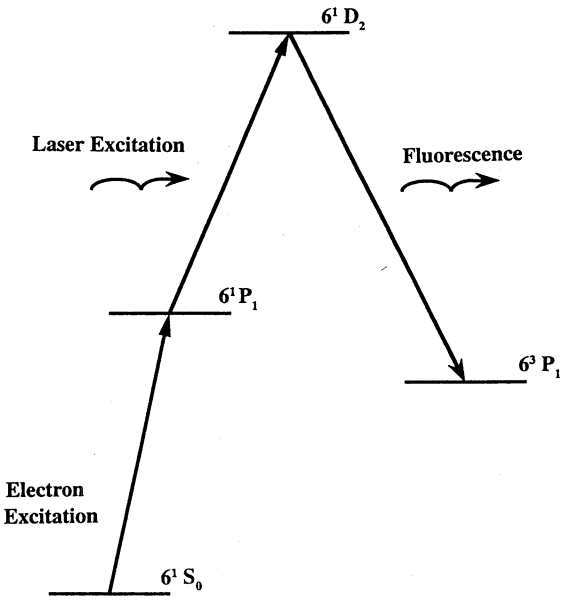

Fig. 5. A stepwise electron–photon excitation scheme in Hg. The target atom is excited by inelastic electron collision from the 6^1S_0 ground state to the 6^1P_1 state, followed by further excitation by resonant laser radiation to the 6^1D_2 state. The fluorescence photon emitted by spontaneous decay in the 6^1D_2–6^3P_1 relaxation channel is detected in coincidence with the scattered electron.

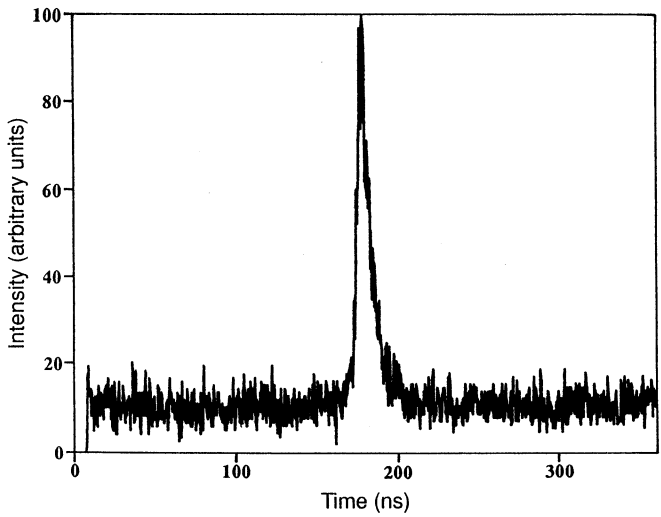

Fig. 6. Time-resolved electron–photon coincidence fluorescence intensity from the 6^1D_2–6^3P_1 transition of Hg derived from the scheme of Fig. 5.

ensemble has reached a time-independent steady state with the radiation before being switched out of resonance with it. It follows from the two-state theory (Brewer 1975) that the time dependence of $\mathrm{Re}[E(t)]$ has the form $\cos(\Delta\omega_{12}t)$, where $\Delta\omega_{12}$ is the Stark shift of the transition frequency produced by the applied voltage pulse.

FID signals from the D_1 line of Na are shown in Fig. 7 as a function of the electric field of the applied voltage (Hannaford *et al.* 1979). To simplify the analysis of the signals, low laser powers were used to greatly reduce the frequency of the optical nutation signal produced by those atoms switched into

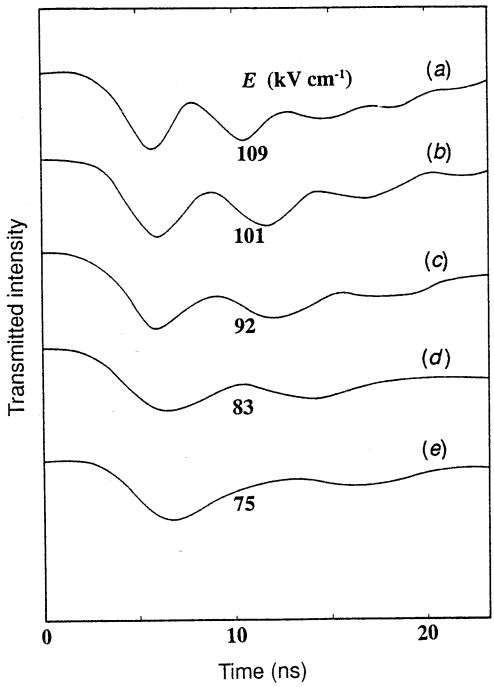

Fig. 7. Coherent optical transient data from the D_1 line of sodium. High-frequency free induction decay oscillations are superimposed on a 10 MHz optical nutation. The values of the imposed electric field are shown. The Stark shift frequencies for each trace are (*a*) 204 MHz, (*b*) 176 MHz, (*c*) 164 MHz, (*d*) 132 MHz and (*e*) 102 MHz. [From Hannaford *et al.* (1979).]

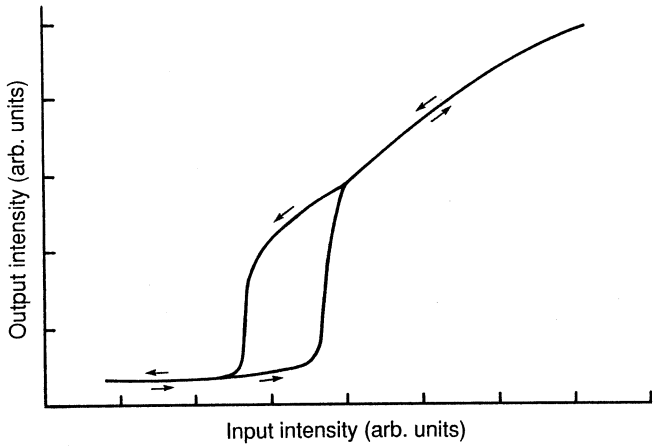

Fig. 8. Hysteresis loop of a bistable system subject to an intensity cycle. The arrows show the direction of change of the intensity.

resonance. In Fig. 7, the high frequency FID signals are superimposed on an optical nutation signal of about 10 MHz. By measuring the frequency of the FID oscillations, the frequency of the transition Stark shift is obtained. This represents a straightforward method of obtaining polarisabilities of atomic levels. In the experiment described above, values deduced for the scalar and tensor polarisabilities for the $3^2P_{\frac{1}{2}}$ and $3^2P_{\frac{3}{2}}$ level of Na were in good agreement with values obtained previously by other, more complicated experimental techniques.

3. Optical Bistability

Optical bistability is the descriptive title given to a class of optical devices which possess two different steady-state transmission states for a given input radiation intensity. The system must have some strongly nonlinear property and the transmission must depend on the output intensity, so that some feedback mechanism is required. In which state the system is found depends on its immediate history, giving rise to a hysteresis cycle (Fig. 8). Gibbs *et al.* (1976) were the first to observe the phenomenon by cyclically varying the intensity of laser radiation injected into a Fabry–Perot etalon containing Na vapour. The appropriate nonlinearity was deduced to be the dispersion of the medium and feedback was achieved by the partially reflecting, partially transmitting output mirror. Other experiments demonstrating dispersive and absorptive optical bistability in atomic Na in Fabry–Perot etalons were subsequently performed (Sandle and Gallagher 1981; Weyer *et al.* 1981).

The interest in optical bistability was not restricted to fundamental research because of the potential of the phenomenon to be applied in the areas of optical communication and optical data processing and storage. Much work has been carried out in developing materials suitable for applications, including semiconductor devices, liquid crystals and interference filters. It is an area of ongoing interest in many laboratories. A definitive text has been produced on the topic (Gibbs 1985).

The theoretical models for optical bistability are based on the Maxwell wave equation [equation (3)] relating the electric field of the radiation to the macroscopic polarisation of the medium, and include appropriate boundary conditions for the cavity. The polarisation is normally calculated from a semiclassical density matrix theory describing the atomic response to the intracavity field. The resultant set of coupled differential equations are referred to as the Maxwell–Bloch equations.

Even though the original experimental work was performed in two-mirror, standing-wave optical cavities (Fabry–Perot etalons), the early theoretical models were developed for ring optical cavities. The internal radiation fields in these devices are travelling waves and, as such, are easier to include in the Maxwell–Bloch equation models than standing waves. If the input mirror is positioned at $z = 0$ and the output mirror at $z = L$, then the boundary conditions for a ring cavity are given by (Lugiato 1983)

$$E(0, t) = T^{\frac{1}{2}} E_{\mathrm{I}}(t) + R \exp(-\mathrm{i}\Delta_{\mathrm{c}} \tau_{\mathrm{R}})\, E(L, t - \Delta t)\,, \tag{14a}$$

$$E_{\mathrm{T}}(t) = T^{\frac{1}{2}} E(L, t)\,, \tag{14b}$$

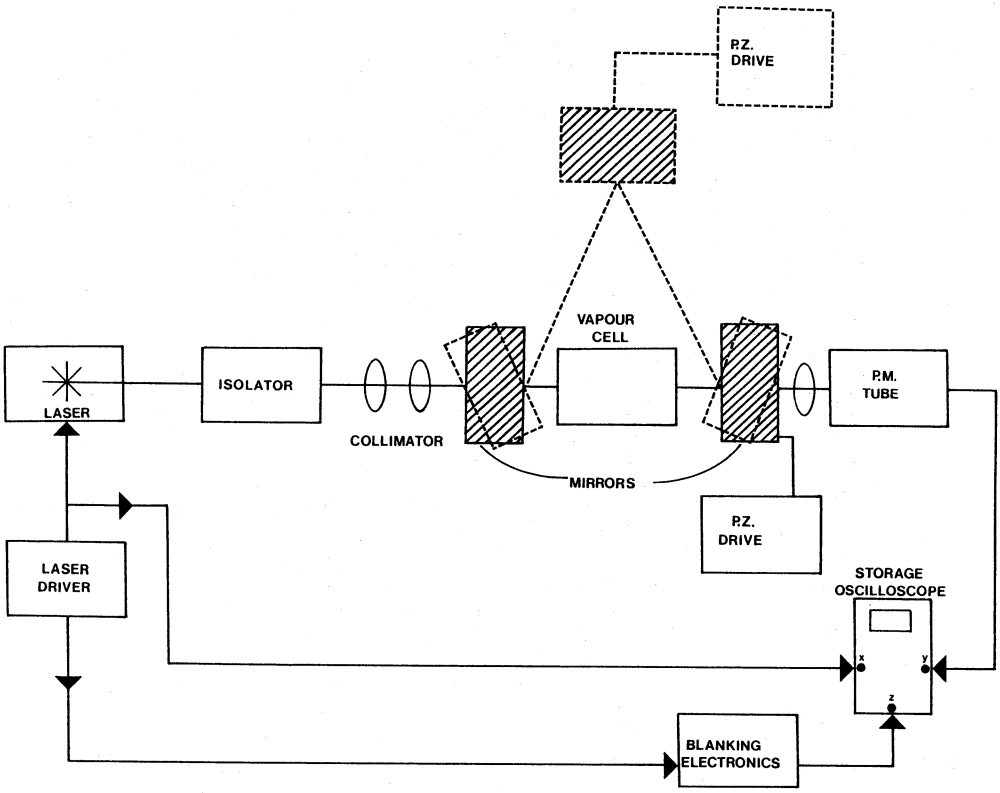

Fig. 9. Schematic diagram of the apparatus configuration for optical bistability experiments using sodium vapour. The dashed lines indicate how the Fabry–Perot etalon can be converted to a three-mirror ring cavity. [From Schulz *et al.* (1983).]

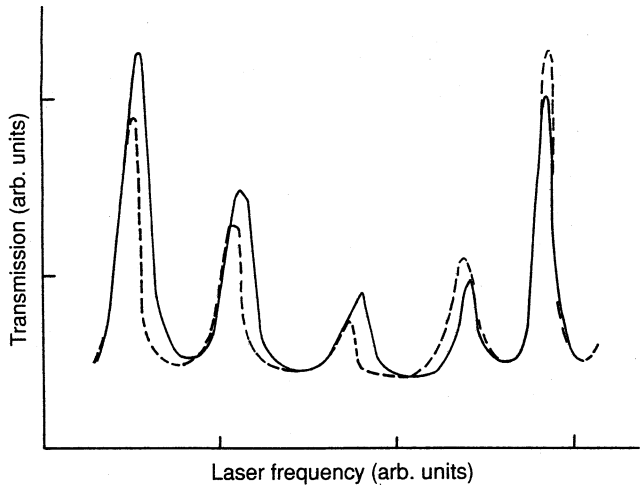

Fig. 10. Transmission of the ring cavity showing optical bistability for the sodium D_1 transition. The low-frequency side is to the right. The solid (dashed) trace represents a sweep to lower (higher) frequency. [From Schulz *et al.* (1983).]

where $E_I(t)$ $[E_T(t)]$ is the incident [transmitted] field amplitude, R (T) is the resistivity (transmittivity) of the input and output mirrors (where the mirrors are assumed to be identical and absorptionless so that $R + T = 1$), Δ_c is the cavity detuning from the radiation and τ_R is the empty cavity round-trip time which is the inverse of the free spectral range.

The first optical bistability experiment performed at Griffith University was to observe the effect in a ring cavity as well as in a Fabry–Perot etalon (Schulz *et al.* 1983). The apparatus for the experiment is illustrated in Fig. 9. Radiation from a Spectra Physics 380A single-mode dye laser was injected into the optical cavity which contained Na vapour as an intracavity medium. The Fabry–Perot etalon consisted of two 93% reflecting, $\lambda/100$ plane mirrors, one of which was mounted in a PZT aligner/translator. The etalon had a free spectral range of 970 MHz and a finesse of about 9. The cavity could be converted to a ring by the addition of one 100% reflecting mirror. The ring cavity also had a finesse of 9 but a free spectral range of 700 MHz. The radiation was linearly polarised in the direction perpendicular to the plane of the ring. The frequency of the laser was scanned and the transmission of the cavity, detected by a photomultiplier tube, was recorded on a storage oscilloscope and photographed. Fig. 10 shows data for the transmission of the ring cavity for laser frequency scanning about the D_1 line. The cavity transmission profiles are distorted due to the switching between the lower and upper branches of the system. The bistable behaviour is evidenced by the observation that the frequency at which the switching occurs in a profile depends on the direction of the frequency sweep. The asymmetry about the centre indicates that the dispersion of the medium is the origin of the bistable behaviour.

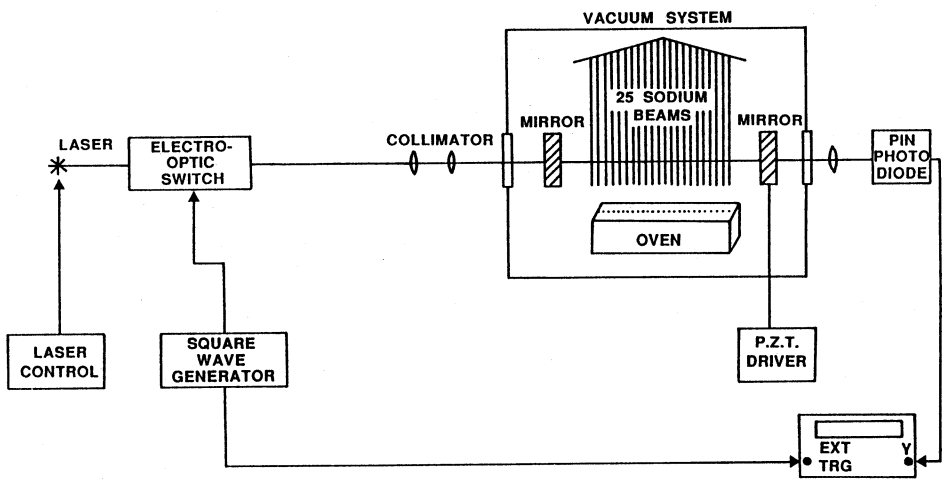

Fig. 11. Apparatus configuration for studying the response of a bistable system to a fast light pulse. The intracavity medium consisted of 25 parallel sodium beams. [From Schulz *et al.* (1989).]

Optical bistability was also observed in a system in which the medium consisted of 25 parallel beams of Na (Schulz *et al.* 1989). A schematic of this apparatus is shown in Fig. 11. The aim of the work with this apparatus was to investigate the response of a bistable system to a fast light pulse. This pulse was formed from cw radiation from an actively stabilised Spectra Physics 380D dye laser by an electro-optic switch. The pulse had a rise time of 1 ns and duration that could be varied between 2 and 480 ns and was passed through a 1 mm aperture so that its intensity profile was reasonably flat. The atomic beam system was contained in a vacuum chamber together with the mirrors which formed either a Fabry–Perot etalon of free spectral range 615 MHz or a ring cavity of free spectral range 1230 MHz. Both cavities had a finesse of about 10. The transmitted light was focused onto a PIN photodiode whose output was recorded on a fast storage oscilloscope.

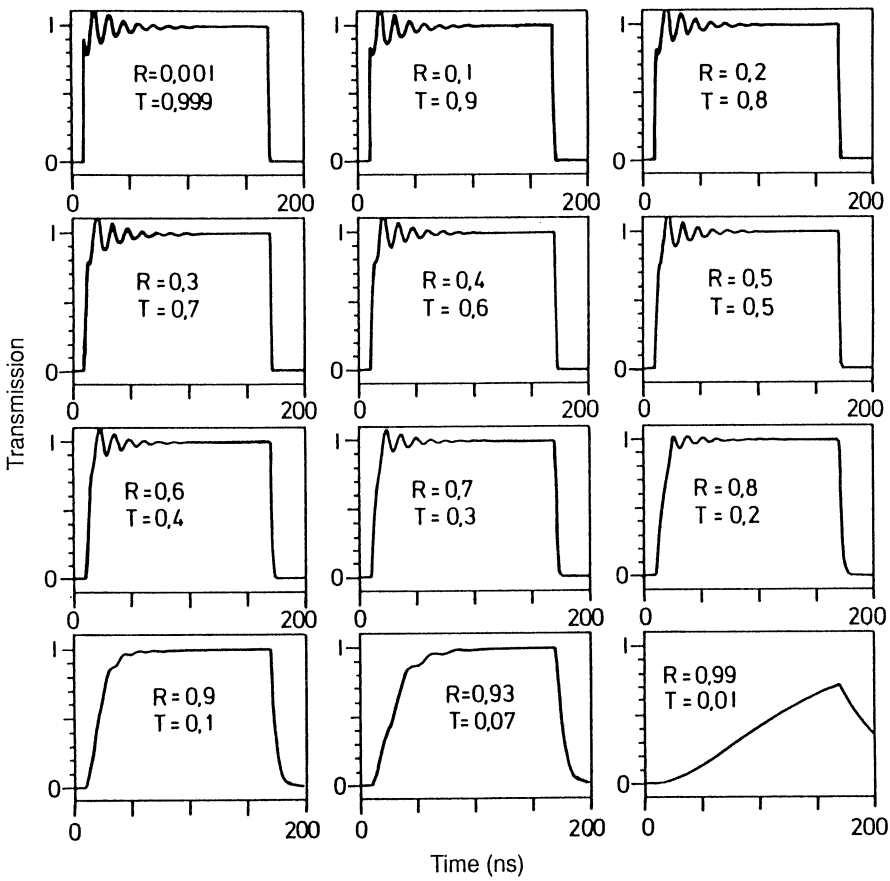

Fig. 12. Simulated response of a ring cavity with a sodium vapour medium to a light pulse with a rise time of 1·5 ns switched on at $t = 10$ ns and off at $t = 170$ ns. The cavity free spectral range is taken as 1200 MHz and the finesse of the cavity is increased from the top left to the bottom right. The intracavity field was kept constant and the system maintained below the threshold for bistability. [From Schulz *et al.* (1989).]

The atomic beams had a residual Doppler width of approximately 200 MHz which was about the same value as the power broadening by the radiation at the intensities used. Thus the ground state transitions from the $F = 2$ and $F = 1$ states of the $3^2S_{\frac{1}{2}}$ level could be resolved, but not the transitions to the hyperfine states of the $3^2P_{\frac{3}{2}}$ level. To facilitate computer simulations of the experiment, the atomic energy level scheme associated with the D lines was approximated to three states of the 'lambda' type with two ground states and one upper state. Further, the dipoles associated with the transitions were taken as equal, as were the branching ratios for the excited state decay. This model for the Na D_2 line had been used previously (Orriols 1979). Confidence in this model was enhanced during the course of this work when it was discovered that the Rabi frequencies observed in optical nutation signals from both the resolved transitions were equal. With this simplified energy level structure and the desirability of invoking a classical field model to facilitate the inclusion of the boundary conditions in the Maxwell equation, semiclassical density matrix models were derived for the bistable systems.

Depending on the characteristic times associated with the optical cavity and the atomic medium, the dynamic response of the bistable system to a light pulse can be dominated by one constituent or the other. For example, in the 'good' cavity limit where a high finesse cavity has a lifetime which is much greater than that of the relevant atomic level, the response of the system is governed by the cavity time evolution, and the atomic response is deemed to follow that of the cavity instantaneously. This allows for the elimination of the time-dependent terms in the equations of motion describing the atomic behaviour. The transient response of such a system to a light pulse has been studied by Kimble's group (Grant and Kimble 1983; Rosenberger *et al.* 1984). Conversely, in a system which has a cavity with a low finesse such that the characteristic time associated with the atomic transition dominates—the 'bad' cavity limit—the response of the atomic medium would be observed. Computer simulations solving equation (3) with the boundary conditions of equation (14) of the response of a ring optical cavity with a sodium vapour medium for various values of finesse are shown in Fig. 12, where the transmitted intensity is plotted as a function of time. The radiation was assumed tuned to the $3^2S_{\frac{1}{2}}(F{=}2)$ to $3^2P_{\frac{3}{2}}(F)$ transition and the cavity was tuned to the radiation. The three-state model for the associated sodium energy levels as described above was employed. The cavity was modelled to have a free spectral range of $1{\cdot}2$ GHz and the intracavity intensity was maintained at a constant value under conditions below that necessary for bistability. The light pulse was assumed to switch on at $t = 10$ ns with a rise time of $1{\cdot}5$ ns and to switch off at 170 ns. The cavity finesse ($F = \pi R^{\frac{1}{2}}/T$) increases from top left to bottom right. For the low values of finesse, optical nutation signals due to the atomic response to the light pulse are clearly evident. However, for the highest finesse, no nutation signal is apparent and the time response is dominated by the slow intracavity radiation filling time.

For the Griffith experiment, the system approached neither the good nor the bad cavity limit, that is, the cavity and atomic lifetimes were approximately equal. The response of the ring cavity system to a 450 ns light pulse tuned approximately to the $3^2S_{\frac{1}{2}}(F{=}2)$ to $3^2P_{3/2}(F)$ transitions is shown in Fig. 13. The data show the transmission of the system versus time for various cavity

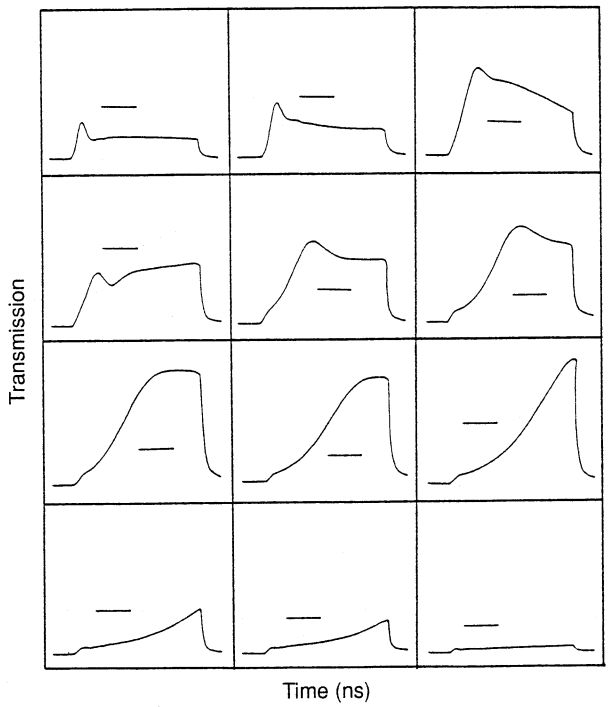

Fig. 13. Response in the transmission of a bistable ring cavity system with an array of sodium beams as its intracavity medium to a light pulse with 1 ns rise time and of 450 ns duration. The free spectral range of the cavity was 1230 MHz. The injected radiation was tuned to the $3^2S_{\frac{1}{2}}(F{=}2)$–$3^2P_{\frac{3}{2}}(F{=}3,2,1)$ transitions of the sodium D_2 line and the cavity tuning was varied in a sequence from top left to bottom right through resonance with the radiation. The length of the dash in each figure is 100 ns. [From Schulz *et al.* (1989).]

frequency settings. Before applying the pulse, it was first established that the system was in a bistable regime in the steady state by cycling the intensity. The tuning range of the cavity was approximately from −150 to 50 MHz (although this parameter could not be measured exactly), ranging from the top left to the bottom right. The best estimate for zero detuning was the profile in the centre of the second bottom row. The asymmetric behaviour of the system about zero detuning indicated that the bistability was dispersive in nature. Analysis of the steady-state curves shows that for the large negative detunings, the system was switching straight on to the upper branch from well above the switch-up threshold. However, as the cavity was tuned closer to resonance with the radiation, the input intensity tended towards the switch-up threshold, resulting in a delay before switching to the upper branch. This delay became greater as the cavity was tuned to positive detuning frequencies until, in the last plot, the system did not switch to the upper branch at all during the pulse, even though still in a bistable regime in the steady state. This phenomenon of long delay in switching when the intensity of the injected radiation is just above the threshold for switch-up is known as critical slowing down, and had previously been observed in good cavity, all-optical bistable systems (Grant and Kimble 1983; Mitschke *et al.* 1983).

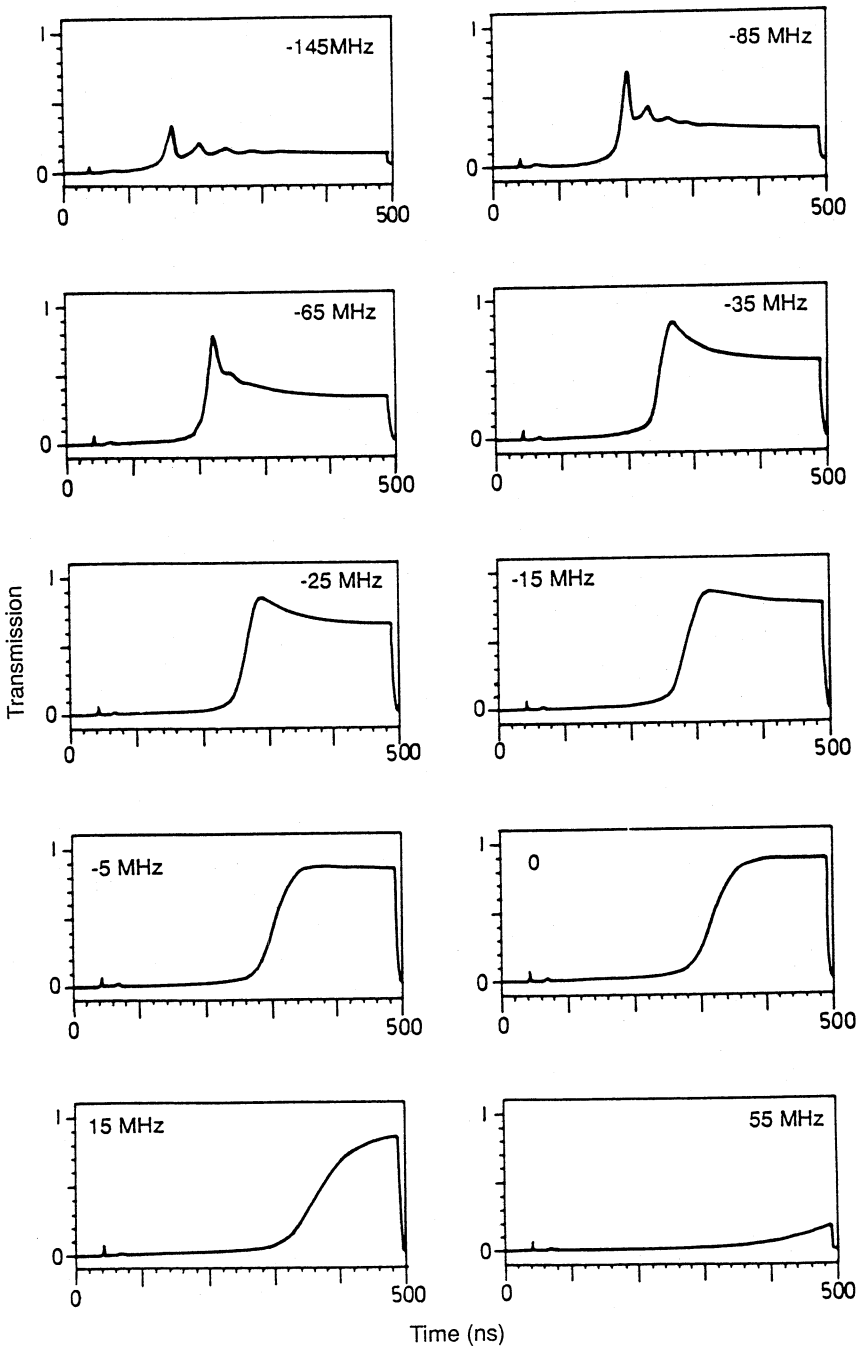

Fig. 14. Simulated ring cavity response for the conditions of the experimental data of Fig. 13. [From Schulz *et al.* (1989).]

Because the bistable system could be described by neither the good nor bad cavity limits, neither the atomic nor the cavity response could be adiabatically eliminated from the Maxwell–Bloch equations of motion (Bonifacio and Meystre 1978). Hence the system of coupled first-order differential equations with the time delay included in equation (14a) had to be solved numerically (Schulz *et al.* 1989). Simulated transmissions for the ring cavity system versus time are shown in Fig. 14, calculated for conditions similar to those of Fig. 13. The qualitative agreement is quite good although the delay in switching is longer in the simulated data. This disagreement may be due to the simplified atomic level structure or the assumption of a flat intensity profile.

During the optical bistability studies, a new phenomenon was discovered (Schulz *et al.* 1983). This effect occurs only in a sodium-vapour-filled Fabry–Perot etalon under conditions below the threshold for bistability. The feature is shown in Fig. 15. The effect occurs in the cavity profile tuned approximately midway between the two ground-state hyperfine transitions. This profile was broadened and split and an enhanced emission peak appeared in the middle of the split peak. The cavity had a free spectral range of about 980 MHz and a finesse of 5. That the effect appeared in a Fabry–Perot etalon and not in a ring cavity suggests that it is due to the motion of the atoms through the standing wave. As well, such an effect had not appeared in the theoretical solution to an ensemble of two-state atoms moving through a standing wave (Carmichael and Agrawal 1980). A density operator model was developed based on the theory of rotating frames (Pegg and Schulz 1985; Schulz *et al.* 1987) which describes an ensemble of three-state lambda configuration atoms moving through a standing wave. It was also necessary for the Doppler broadened transitions from the ground states to overlap as indeed is the case for sodium atoms in a vapour. This condition was necessary so that there could be a velocity class of atoms which, due to their motion and detuning, could have the radiation propagating in one direction Doppler tuned to one transition from the ground states, while the counter-propagating radiation is Doppler tuned to the other transition. It is the same velocity group that gives rise to the well-known 'cross-over resonances' observed in saturation absorption spectroscopy (see, for example, Levenson and Kano 1988). In the atomic beam system as described above, this feature was not observed due to the fact that the ground state transitions were resolved. Subsequently, it was deduced that a four-state model for the sodium atom under the conditions of this experiment was more appropriate (MacGillivray and Pegg 1988). In this model, the two ground states are each excited simulataneously to two orthogonal upper states. The simulation with this model is shown in Fig. 16. The agreement between the theoretical calculation and the experimental data is very good.

The theoretical modelling showed that the narrow, enhanced emission feature of Fig. 15, the so-called 'central feature', occurred at an absolute frequency slightly detuned from the frequency midway between the two ground state transitions. The slight asymmetry in the system was due to the unequal branching ratios in the cross-relaxation channels. An absolute frequency is always attractive for use in standards but, in this case, the width of the feature was too great. The theoretical models predicted that the central feature would be observed only for a small range of parameters of atom density, radiation intensity and cavity finesse and free spectral range, highlighting how fortuitous was its observation.

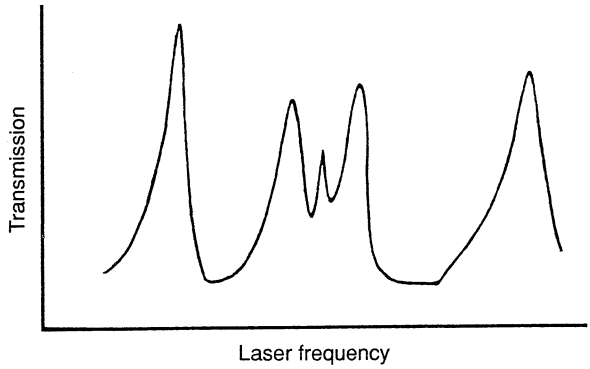

Fig. 15. Experimental data for the absolute-frequency central feature in the transmission of a Fabry–Perot etalon filled with sodium vapour under conditions below threshold for bistability. See text for details.

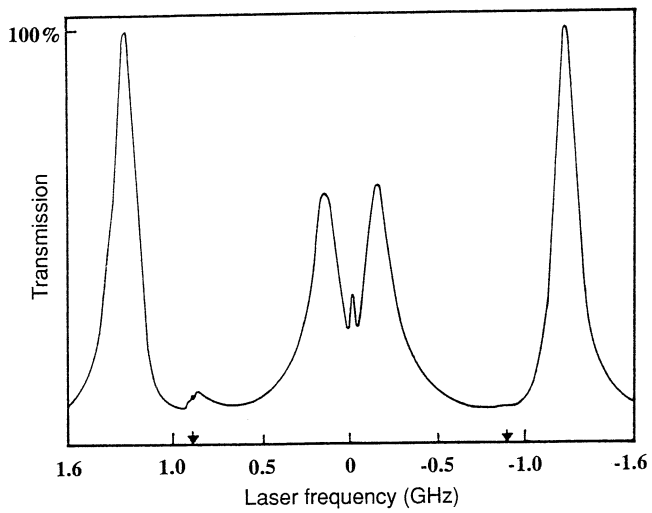

Fig. 16. Simulation of the central feature using a four-state model. The horizontal axis is calibrated in terms of the detuning of the laser frequency from the midpoint between the two ground-state transitions, which are indicated by an arrow.

4. Atom Manipulation by Light

There is currently considerably activity in developing methods of atom cooling and trapping and other forms of manipulation using light or a combination of light and magnetic fields. Several popular reviews have been written on the topic recently (see, for example, Cohen-Tannoudji and Phillips 1990; Chu 1992 and references therein). In the Australian context, there are four groups known to be actively pursuing research in this area. Both the Australian National University and the Melbourne University/CSIRO Division of Materials Science and Technology groups are developing atomic interferometers by different methods and a group at the CSIRO Division of Applied Physics is constructing an ion trap

apparatus for frequency standards experiments. At Griffith University, the work is concentrating on the information obtainable by detecting atoms in a beam that have been deflected by a laser propagating at right angles to the beam.

To describe the deflection process in physical terms, we consider the interaction between an atom in the beam and resonant laser radiation. The atom absorbs a photon then, as observed directly in the optical nutations described in Section 2, it can be stimulated by the radiation to emit a photon. Because stimulated emission is a coherent process, the photon will be emitted in the same direction as the radiation and so there will be no net change in the momentum transferred to the atom. However, when the atom relaxes due to the incoherent spontaneous decay process, the photon can be emitted in any direction with equal probability. After several events of absorption followed by spontaneous emission, there will be a net transfer of momentum to the atom in the direction of propagation of the radiation. This is the principle behind cooling atoms with radiation propagating in the direction opposite to that of the atomic motion. If the laser beam is at right angles to the atomic beam, the interaction will result in a deflection of the atoms.

In a uniform travelling laser field, the expectation value of the deflection force $\langle \boldsymbol{F}(t) \rangle$ for resonant interaction between the radiation and an ensemble of atoms is given by (Ungar *et al.* 1989)

$$\langle \boldsymbol{F}(t) \rangle = -\mathrm{i}\,\hbar k \sum_{\mathrm{eg}} [\tilde{\rho}_{\mathrm{ge}}(t) - \tilde{\rho}_{\mathrm{eg}}(t)] \frac{\Omega_{\mathrm{eg}}}{2}\,, \tag{15}$$

where k is the wave vector of the radiation, Ω_{eg} is the Rabi frequency of the transition between states $|\mathrm{g}\rangle$ and $|\mathrm{e}\rangle$, and $\tilde{\rho}_{\mathrm{ge}}(t)$ and $\tilde{\rho}_{\mathrm{eg}}(t)$ are the slowly varying components of the density matrix, suitably averaged over the ensemble, which describe the optical coherences. The momentum transferred to the atoms by this force in the time interval $t = 0$ to t, where the laser–atom interaction commences at $t = 0$, is written as

$$\langle \boldsymbol{P}(t) \rangle = \sum_{mn} \alpha_{mn}(t)\, \tilde{\rho}_{mn}(0)\,. \tag{16}$$

That is, the transferred momentum, and hence the atomic deflection, depends on the value of the density matrix at the time the atoms enter the laser beam. The terms $\alpha_{mn}(t)$ describe the optical pumping of the atom by the radiation, and are calculated using the full QED model discussed in Section 2. For single-mode excitation in the reference frame defined by the laser polarisation, that is, the direction of propagation for circular polarisation and the direction of the electric field vector for linear polarisation, the only initial-state density matrix elements on which the momentum depends are the ground-state population terms $\rho^{\mathrm{L}}_{\mathrm{gg}}(0)$, where the superscript denotes the laser frame. A deflection measurement would yield information on the initial distribution of population among the ground-state substates. However, the initial ground-state population elements, $\rho^{\mathrm{L}}_{\mathrm{gg}}(0)$, are related to the elements of any other frame, $\rho^{\mathrm{P}}_{\mathrm{g'g''}}(0)$ say, by (Blum 1981)

$$\rho^{\mathrm{L}}_{\mathrm{gg}}(0) = \sum_{\mathrm{g'g''}} D^{J}_{\mathrm{g'g}}{}^{*}(\omega)\, D^{J}_{\mathrm{g''g}}(\omega)\, \rho^{\mathrm{P}}_{\mathrm{g'g''}}(0)\,, \tag{17}$$

where $D^J_{g''g}(\omega)$ is an element of the operator which describes the rotation from the laser frame to the other frame through Euler angles ω (Edmonds 1974). It can be seen from equation (17) that if the atoms have been prepared by some process in a frame other than the laser excitation frame, then a deflection measurement will contain information about off-diagonal (superposition state) as well as diagonal (population) density matrix elements in the P or preparation frame.

Further, by selecting various geometrical arrangements and then determining the ground-state population terms in the laser excitation frame by atomic deflection measurements for each, complete information about the preparation of the atom may be obtained including superposition states. Recently, it has been demonstrated that it is possible to obtain information about a state population distribution from atom deflection by resonant laser photons (Kaiser *et al.* 1991). In this experiment, the deflection of He 2^3S_1 metastable atoms by laser radiation of fixed polarisation as a function of applied magnetic field was measured, yielding a so-called 'mechanical Hanle effect'.

We intend to use the deflection technique to study inelastic collisions between electrons and atoms, in particular, electron excitation of metastable states in atoms (Summy *et al.* 1992). Information about the differential cross sections (populations) and the amplitudes and relative phases of the electron scattering should be obtained by measuring the atomic deflection after the collision using appropriate laser polarisation settings. Extensive theoretical modelling has been performed and a pilot experiment is currently in progress. Deflections of Na atoms of the order of 10 mm in $1 \cdot 2$ m travel after the laser interaction have been observed. Theoretical work has also predicted that deflection by a dispersion process may be more sensitive although the specifications of the experiment are more stringent. We are considering this method further.

5. Conclusion

We have reviewed three areas of investigation into resonant laser–atom interaction which have been or are currently being undertaken. In all of the studies described, the experimental data have been supported by simulated data from theoretical models. The most sophisticated of these models is the full quantum-electrodynamic description which has been developed to be generally applicable. This theoretical approach has been tested not only by explaining the data from experiments included here, but also in other detailed tests (Meng *et al.* 1992).

In principle, the QED model should be employed to describe resonant laser radiation excitation of atomic transitions at all times, but there are practical limits in terms of the computing facilities available. The best example in the work reviewed was for optical bistability, where using the full 24-state model for the sodium D_2 line in the Maxwell–Bloch equations for a Doppler-broadened medium inside a ring cavity, let alone the standing-wave cavity of a Fabry–Perot etalon, was a numeric and computing impossibility. In these circumstances, it was shown that good qualitative agreement between the data and a semiclassical density matrix theoretical model with a simplified atomic state structure for sodium could be obtained. This enabled explanation of all of the phenomena observed, including the unpredicted central feature.

Fundamental to all models of resonant radiation excitation of atoms is the need for a detailed knowledge of the Rabi frequencies for the associated transitions. This is particularly true when non-degenerate energy states are involved, as both the amplitude and the phase of the Rabi frequency must be included in the model to describe correctly the quantum interference effects. There are several known methods for calculating values for the Rabi frequency and, until recently, there appeared to be disagreement in the relative phases produced by each within a manifold of transitions. However, this inconsistency has recently been removed and calculations of the Rabi frequency can now proceed with confidence using any of the methods (Farrell *et al.* 1994).

Research in the areas of atomic spectroscopy and quantum optics is still a fertile ground. In the last two decades, new topics such as optical bistability, multiphoton processes, squeezed states, quantum non-demolition measurements and now atom cooling and manipulation have made enormous impacts both within and beyond the atomic physics community. In the field of collision physics, the use of resonant excitation by laser radiation to enable a more detailed understanding of the scattering processes, as well as the performance of new experiments, is becoming more widespread. There is much more work to be done.

Acknowledgments

We wish to acknowledge financial support from the Australian Research Grants and Griffith University Research Grants Schemes, as well as the Australian Research Council and the School of Science, Griffith University. We also acknowledge the following people, Werner Schulz, Andrew Murray, Peter Farrell, Gil Summy, Peter Hannaford, David Pegg and Peter Knight, for their contributions to the work described in this article. We also recognise the indispensible work of the workshops of the Faculty of Science and Technology, Griffith University.

References

Ackerhalt, J. R., and Eberly, J. H. (1974). *Phys. Rev.* D **10**, 3350.
Ackerhalt, J. R., Knight, P. L., and Eberly, J. H. (1973). *Phys. Rev. Lett.* **30**, 456.
Allen, L., and Eberly, J. H. (1975). 'Optical Resonance and Two-level Atoms' (Wiley: New York).
Blum, K. (1981). 'Density Matrix Theory and Applications' (Plenum: New York).
Bonifacio, R., and Meystre, P. (1978). *Optics Commun.* **27**, 147.
Brewer, R. G. (1975). *In* 'Frontiers in Laser Spectroscopy' (Eds R. Balian *et al.*), p. 339 (North Holland: Amsterdam).
Brewer, R. G., and Shoemaker, R. L. (1971). *Phys. Rev. Lett.* **27**, 631.
Carmichael, H. J., and Agrawal, G. P. (1980). *Optics Commun.* **34**, 293.
Chu, S. (1992). *Scient. Am.* **266**, 49.
Cohen-Tannoudji, C., and Phillips, W. D. (1990). *Phys. Today* **43**, 33.
Edmonds, A. R. (1974). 'Angular Momentum in Quantum Mechanics' (Princeton Univ. Press).
Farrell, P. M., MacGillivray, W. R., and Standage, M. C. (1985). *Phys. Lett.* **107**, 263.
Farrell, P. M., MacGillivray, W. R., and Standage, M. C. (1988). *Phys. Rev.* A **37**, 4240.
Farrell, P. M., MacGillivray, W. R., and Standage, M. C. (1994). In preparation.
Gibbs, H. M. (1985). 'Optical Bistability: Controlling Light with Light' (Academic: Orlando).
Gibbs, H. M., McCall, S. L., and Venkatesan, T. N. C. (1976). *Phys. Rev. Lett.* **36**, 1135.
Grant, D. E., and Kimble, H. J. (1983). *Optics Commun.* **44**, 415.
Hannaford, P., MacGillivray, W. R., and Standage, M. C. (1979). *J. Phys.* B **12**, 4033.
Kaiser, R., Vansteenkiste, N., Aspect, A., Arimondo, E., and Cohen-Tannoudji, C. (1991). *Z. Phys.* D **18**, 17.

Knight, P. L., and Allen, L. (1983). 'Concepts of Quantum Optics' (Pergamon: Oxford).
Levenson, M. D., and Kano, S. S. (1988). 'Introduction to Nonlinear Laser Spectroscopy' (Academic: San Diego).
Lugiato, L. A. (1983). *Contemp. Phys.* **24**, 333.
MacGillivray, W. R., and Pegg, D. T. (1988). *Optics Commun.* **66**, 299.
MacGillivray, W. R., Pegg, D. T., and Standage, M. C. (1978). *Optics Commun.* **25**, 355.
MacGillivray, W. R., Standage, M. C., Farrell, P. M., and Pegg, D. T. (1990). *J. Mod. Optics* **37**, 1741.
Meng, X.-K., MacGillivray, W. R., and Standage, M. C. (1992). *Phys. Rev.* A **45**, 1767.
Mitschke, F., Deserno, R., Mlynek, J., and Lange, W. (1983). *Optics Commun.* **46**, 135.
Murray, A. J., MacGillivray, W. R., and Standage, M. C. (1991). *J. Mod. Optics* **38**, 961.
Orriols, G. (1979). *Nuovo Cimento* B **53**, 1.
Pegg, D. T., and Schulz, W. E. (1985). *Optics Commun.* **53**, 274.
Rosenberger, A. T., Orozco, L. A., and Kimble, H. J. (1984). *In* 'Fluctuations and Sensitivity in Nonequilibrium Systems' (Eds W. Horsthemke and D. K. Kondepudi), p. 62 (Springer: Berlin).
Sandle, W. J., and Gallagher, A. (1981). *Phys. Rev.* A **24**, 2017.
Schulz, W. E., MacGillivray, W. R., and Standage, M. C. (1983). *Optics Commun.* **45**, 67.
Schulz, W. E., MacGillivray, W. R., and Standage, M. C. (1987). *Phys. Rev.* A **36**, 1316.
Schulz, W. E., MacGillivray, W. R., and Standage, M. C. (1989). *Aust. J. Phys.* **42**, 267.
Summy, G. S., MacGillivray, W. R., and Standage, M. C. (1992). Abstracts 13th Int. Conf. on Atomic Physics, C20.
Ungar, P. J., Weiss, D. S., Riis, E., and Chu, S. (1989). *J. Opt. Soc. Am.* B **6**, 2059.
Weyer, K. G., Wiedenmann, H., Rateike, M., MacGillivray, W. R., Meystre, P., and Walther, H. (1981). *Optics Commun.* **37**, 426.

Manuscript received 14 December 1992, accepted 1 September 1993